Highly Sensitive Terahertz Metasurface Based on Electromagnetically Induced Transparency-Like Resonance in Detection of Skin Cancer Cells

Shohreh Nourinovin, *Member, IEEE,* Muhammad M Rahman, Mira Naftaly, Michael P Philpott, Qammer H Abbasi, *Senior Member, IEEE* Akram Alomainy, *Senior Member, IEEE,*

***Abstract*—Terahertz (THz) metasurfaces based on high Q-factor electromagnetically induced transparency-like (EIT-like) resonances are promising for biological sensing. Despite this potential, they have not often been investigated for practical differentiation between cancerous and healthy cells. The present methodology relies mainly on refractive index sensing, while factors of transmission magnitude and Q-factor offer significant information about the tumors. To address this limitation and improve sensitivity, we fabricated a THz EIT-like metasurface based on asymmetric resonators on an ultra-thin and flexible dielectric substrate. Bright-dark modes coupling at 1.96 THz was experimentally verified, and numerical results and theoretical analysis were presented. An enhanced theoretical sensitivity of 550 GHz/RIU was achieved for a sample with a thickness of $13\mu m$ due to the ultra-thin substrate and novel design. A two-layer skin model was generated whereby keratinocyte cell lines were cultured on a base of collagen. When NEB1-shPTCH (basal cell carcinoma (BCC)) were switched out for NEB1-shCON cell lines (healthy) and when BCC's density was raised from 1×10^5 to 2.5×10^5, a frequency shift of 40 and 20 GHz were observed, respectively. A combined sensing analysis characterizes different cell lines. The findings may open new opportunities for early cancer detection with a fast, less-complicated, and inexpensive method.**

***Index Terms*—Terahertz, Metasurface, EIT-like resonance, Early cancer detection**

I. Introduction

Non-melanoma skin cancers including basal cell carcinoma (BCC) and squamous cell carcinoma (SCC) have been alarmingly on the rise for the past 30 years. Visual examination, electrical impedance spectroscopy (EIS), high-frequency ultrasonography (HFUS), and optical coherence tomography (OCT) are some of the current methods used to examine skin cancer. These are typically either costly, time consuming and require complicated pre-processing or are invasive due to high-frequency ionization impact [1]. Unlike short-wavelength technologies, THz waves have lower photon energy without ionization effect on the tissues. Moreover, due to the considerable absorption of THz waves by hydrogen bonds in water and the higher water content of tumors than normal tissue [2], it is widely studied as ideal non-invasive spectroscopy, and imaging for early cancer detection [3]–[5].

Despite recent impressive THz spectroscopy and imaging advancements, it still struggles with low sensitivity and contrast in practical applications. These flaws give a great opportunity to THz metasurfaces-enhanced biosensors. Electromagnetic (EM) metasurfaces are artificial structures frequently constructed using resonators with a size scale smaller than the wavelength of the illuminating light. The incident stimuli travel through the resonators' surface and pair with their surface current. As a result, the analyte's interaction with the interrogating field is strengthened locally, and the biosensor's sensitivity dramatically increases, reflected in resonance frequency, transmission magnitude, and Q-factor. Thus, they have been widely studied for biological sensing [6], [7] including sensing glucose [8], Citrate salt [9], ethanol [10], insulin [11] and viruses [12]. There are also various strategies for tuning metasurfaces based on mechanical reconfiguration and combined with active materials including varactor diodes, semiconductors, liquid crystals, phase change materials, superconductors, and two-dimensional materials [13].

Many studies have developed ultrasensitive THz biosensors for cancer detection using different higher order plasmonic modes in metasurfaces [14], including classical plasmonic [15]–[17], extraordinary transmission [18], [19], nano-particle-enhanced [8], graphen-enhanced [20], toroidal [21] and Fano and EIT-like metasurfaces [22]. A detailed table of comparison, can be found in our recent survey [14].

Designing high Q-factor metasurfaces with increased sensitivity is essential for thin-film biological sensing. An ohmic loss in THz resonant-based metasurfaces is frequently insignificant due to small interaction length of radiation with metal. Also, in dielectric-based metasurfaces, selecting the proper substrate results in minimizing further losses. Therefore, the key issue that needs to be addressed to improve the Q-factor is radiation losses. Higher-order plasmonic modes, such as Fano and EIT-like resonance-based metasurfaces [23] [24], can be employed to fulfill this requirement and have been widely studied for biosensing [25]. A number of research works have investigated using THz EIT-like metasurfaces for experimentally detecting the different concentrations of cancer cells [26]–[28].

Ref [26] worked on an EIT-like metasurface based on cut-wire and SRRs to detect various lung cancer cells of

Sh.Nourinovin and A.Alomainy are with the School of Electronic Engineering and Computer Science, Queen Mary University of London, London E1 4FZ, U.K. (e-mail:s.nourinovin@qmul.ac.uk; a.alomainy@qmul.ac.uk), M.M.Rahman and M.P.Philpott are with the Centre for Cell Biology and Cutaneous Research of Blizard Institute, Queen Mary University of London, London E1 2AT, U.K. (e-mail: m.m.rahman@qmul.ac.uk; m.p.philpott@qmul.ac.uk), Q.H.Abbasi is with the James Watt School of Engineering, University of Glasgow, Glasgow, G12 8QQ, the U.K. and the School of Electronic Engineering and Computer Science, Queen Mary University of London, London E1 4FZ, U.K. (e-mail: Qammer.Abbasi@glasgow.ac.uk)

different concentrations with a theoretical sensitivity of 248.8 GHz-RIU. Following that, Yang et al. [27] designed an EIT-like THz metasurface based on asymmetric structures with a theoretical sensitivity of 455.7 GHz/RIU for sensing the different concentrations of oral cancer along with the effect of anticancer drugs. Another study [28] presented an EIT-like metasurface with a theoretical sensitivity of 496.1 GHz/RIU in detecting glioma cells of differentecdie aggressiveness.

However, most of these studies only consider resonance frequency shift, whereas working with complex biological samples like cancer cells necessitates a more thorough study that also considers changes in both the transmission magnitude and full width at half maximum (FWHM). These variables are crucial in defining the characteristics of cancer cells. Besides, the ability of the biosensor to distinguish between healthy and malignant tissue also plays a critical part in the early detection of cancer, despite the fact that the previous works mostly concentrated on featuring varying concentrations of cancer cells. Last but not least, higher sensitivity produces more precise results, and there is a demand for more novel designs to suppress losses and obtain more sensitive metasurfaces. The current manuscript offers improved theoretical sensitivity [27], [28] and, unlike conventional refractive-index-based metasurfaces, utilizes a combinational sensing mechanism, which measures not only the reaction to an increased concentration of cancer cells [15], [18], [29] but also the contrast between normal and tumor cells.

Human skin is formed of two main layers, which are the epidermis and dermis, that act as outer and inner layers, respectively. The epidermis is made up of flat, scale-like cells known as keratinocytes, created by the gradual maturation and differentiation of basal cells, which originate at the basal layer of the epidermis. BCC is the lesion that results from the uncontrolled growth of abnormal basal keratinocytes cells. Recent organotypic cell culture technology that employs 3D gel-based techniques enables more complex studies that better mimic skin. 3D tissues, as opposed to 2D culturing resemble in vivo environment more closely in terms of morphology and physiology, and provide more precise tumour information and features, as keratinocytes are able to grow in 3D.

In this work, we have designed a flexible EIT-like metasurface based on asymmetric SRRs fabricated on an ultra-thin and flexible substrate. An anti-parallel surface current arises in a closed loop because the quadrupole mode is excited, and by suppressing radiation losses, a transparency window developed at the frequency of 1.96 THz with a transmission peak magnitude of 0.8. The structure was fabricated with four asymmetry levels to measure the intensifying trend of EIT-like resonance. The coupled harmonic oscillator model is investigated to theoretically extract the damping rates and coupling coefficients of various asymmetry values in addition to the EM fields and surface current analysis. For different sample characteristics, a combined analysis based on resonance frequency, transmission magnitude, and FWHM variations was established. By modeling a sample with a thickness of 13 μm and a refractive index of 1.6 in the frequency range of 0.5 to 2.5 THz, an enhanced theoretical sensitivity of 550 GHz/RIU and a Q-factor of 5.13 were achieved. On a layer of collagen, which serves to mimic the skin's dermis layer, we grew NEB1-shCON (normal) and NEB1-shPTCH1 (BCC) immortalised keratinocyte cells to test the experimental sensitivity. A frequency shift of 40 and 20 GHz was seen when BCC was replaced by normal keratinocytes and when the BCC cell number was increased from 1×10^5 to 2.5×10^5, respectively. To characterize cancer cells, a combined analysis of the transmission magnitude, frequency shift, and FWHM variation was conducted. The results demonstrate the viability of the designed metasurface as a fast, affordable, flexible, and sensitive device for skin cancer detection.

II. Design, Fabrication and Cell Culture Methods

The unit cell of the designed metasurface consists of two asymmetric metallic split-ring resonators on top of a dielectric layer, illustrated in Fig. 1. The metal layer is made of gold with a conductivity of $4.461 \times 10^7 s/m$. The material of the dielectric layer is polyimide with a thickness of $6\mu m$, a permittivity of 2.9, and a loss tangent of 0.05 at 1 THz. With the low permittivity and dissipation loss, this ultra-thin substrate used for THz metasurfaces offers both mechanical support and a high Q-factor [30]. Another benefit of employing this substrate is that it is flexible, which reduces numerous obstacles in practical biosensing applications [31].

The incident THz waves interact with the gold metallic pattern and pass through the dielectric layer. The detailed dimensions of the unit cell geometries can be seen in the caption of Fig. 1. The parameter d represents the asymmetry value between the coupled resonators which will be used for tuning the EIT-like resonance. The metasurface resonance response is simulated and optimized by the CST microwave studio software based on a finite difference time domain (FDTD) solver. For the polarization of the incident EM wave, as shown in Fig.1, the electric, magnetic and open (add space) boundary conditions are considered along x , y and z direction, respectively.

The metasurface sensor was fabricated using several processing steps. First, a polyimide layer was spin coated and baked on a silicon wafer. Following the polyimide coating, a bilayer of photoresist was spin-coated onto the polyimide. The photoresist was exposed using a Heidelberg uPG 101 direct laser write system. Metasurface was patterned and developed using maskless laser lithography and conventional developing process, respectively. A Ti/Au metal adhesion layer with thickness of 20 nm/180 nm was deposited using a sputter coater. To release the polyimide layer, the wafer was immersed in 48% hydrofluoric acid for 30 minutes and rinsed in deionized water to remove the Si_O2 layer. The polyamide was then peeled from the wafer using tweezers. The final fabricated metasurface was $6.3 \times 6.3\ mm$ in size with an array of 90×90 unit cells. The flexibility of the fabricated biosensor can be observed in Fig. 2. (a). The image of the final metasurface biosensor under an optical microscope is depicted in Fig.2. (b-c).

To generate a 3D-skin model, we first made a dermis base layer of 200 μml human collagen type I which was allowed to solidify in a 24-well plate. Once set, NEB1 immortalised keratinocytes cell lines of NEB1-shCON (normal

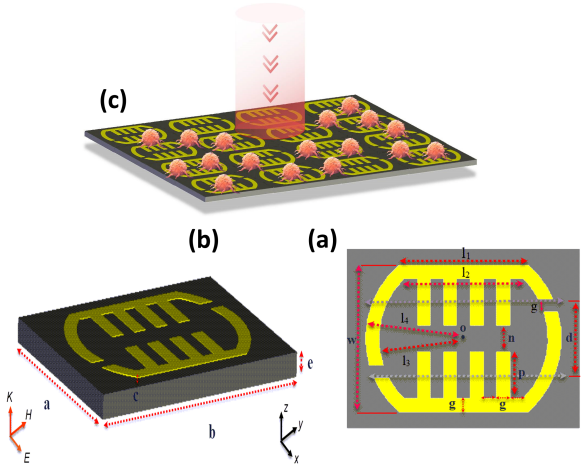

Fig. 1: Schematic illustration of the unit cells of the designed metasurface biosensor. (a) top view of the unit cell with the circle center of O with the following parameters: $l_1 = 39\ \mu m$, $l_2 = 36\ \mu m$, $l_3 = 25.45\ \mu m$, $l_4 = 29.45\ \mu m$, $g = 4\ \mu m$, $n = 8\ \mu m$, $p = 14\ \mu m$, $d = 20\ \mu m$, $w = 44\ \mu m$, (b) side view of the unit cell with following parameters: $a = b = 70\ \mu m$, $c = 0.2\ \mu m$, $e = 5\ \mu m$ (c) arrays of coupled resonators with THz beams normally incident through the biosensor on which the skin cancer sample was placed.

keratinocytes) and NEB1-shPTCH (BCC model) [32] were cultured on top of the collagen gels at two different densities (1×10^5 and 2.5×10^5) for 48 hours. All cells were cultured in DMEM/Ham's F12 (Gibco) supplemented with 10% (v/v) heat-inactivated foetal bovine serum (FBS) (Lonza), 2% (v/v) penicillin-streptomycin (PAA Laboratories), 2 nM L-glutamine and RM+ supplement containing 0.5 $\mu g/ml$ hydrocortisone, 5 $\mu g/ml$ insulin, 10 ng/ml epidermal growth factor (EGF), 5 $\mu g/ml$ transferrin, 9.2×10^{-4} M liothyronine and 1×10^{-10} M cholera toxin (Sigma). The keratinocytes were seeded on top of the gel. The cultured cells in a 24-well plate and an image of the final BCC tissue can be seen in Fig. 2. (d-e). After 48 hours, the 3D gels were washed with PBS (Gibco) then fixed with 70% ethanol for 1 hour at 4°c before analysis with the biosensor. For the measurements, a terahertz time-domain spectroscopy system (THz-TDS) in transmission mode was used to record transmission spectra in the frequency range of 0.1 to 4 THz. TDS measurements were carried out using a TeraFlash Pro spectrometer from Toptica Photonics set up in a standard optical configuration with four F/2 parabolic mirrors. The THz beam path was purged with dry air to eliminate absorption from atmospheric water vapor. Samples were placed normal to the beam axis in the focal plane of the beam, where the beam diameter was $< 3mm$. The frequency resolution was 10 GHz.

III. Simulation, Theory and Measurement Results and Discussion

The coupling between the bright and dark resonators occurs when the asymmetry degree of d applies, which breaks the resonance equilibrium in the close-by arms. The brown and black graphs of Fig.3. (a-d) show the EM simulation and measured transmission spectra of the structures with four asymmetry values of 16, 20, 24, and $28\mu m$. The simulations and measurements are in good agreement except for a slight difference related to fabrication error. The peak of the EIT-like resonance occurs at 1.96 THz due to the coupling of the bright and dark modes. As can be observed, with increasing the asymmetry degree d from 16 to 28 μm (Fig. 3. (a-d)), the coupling strength between the resonators increases gradually and the peak transmission intensifies resulting in a quadruple EIT-like mode with narrow linewidth and strong transmission window [33]. According to the theory of the EIT-like effect, [34], the resonator considered as the bright (radiative) mode interacts with the propagating EM waves while the dark resonator (non-radiative) is uncoupled with the external waves. In the absence of coupling between the bright and the dark modes, the energy excited by the external wave in the bright mode is scattered into free space or absorbed in the radiative mode, and transmission falls at the resonant frequency. When two asymmetric resonators are coupled with each other, transparency window occurs, and the energy received through the bright mode is effectively transferred into the dark mode for excitation waves at the resonant frequency of 1.96 THz. The mutual magnetic coupling between the two resonators gives rise to an effective magnetic dipole moment that is oriented perpendicular to the metasurface plane. As a result, the absorption or scattering loss is significantly suppressed due to the dark mode's small dissipation. Although the design with an asymmetry value of 28 μm has a higher transmission peak than 24 μm, it suffers from a lower Q-factor, so by considering a trade-off between these two values, the design with an asymmetry value of 24 μm is considered for the rest of the study.

In order to analyze the EIT-like effect, the electric and magnetic field, as well as the current distribution of the structure, is depicted at the two resonance dips of f_1 and f_3, and the transmission peak of f_2 in Fig. 4. (a-d). According to Fig. 4 (b), at the frequency of f_1, there is a direct dipole excitation of the bright mode from the incident wave while coupling with the free space. In the meantime, an incomplete semi-circulating current is generated on each side of the resonator pairs and leads to a weak magnetic field. At the frequency of f_2, as illustrated in Fig. 4 (c), destructive interference and a suppressed state in the bright resonator take place. In response to the excitation of the quadrupole mode, a strong magnetic dipole forms between coupled resonators leading to antiparallel surface currents in a closed loop. At this frequency, a transparency window formes, and radiative losses are suppressed; therefore, the EIT-like Fano resonance of the structure only depends on the non-radiative damping, such as loss in the metallic structure. This remarkable characteristic makes it possible to build an ultra-sensitive biosensor since

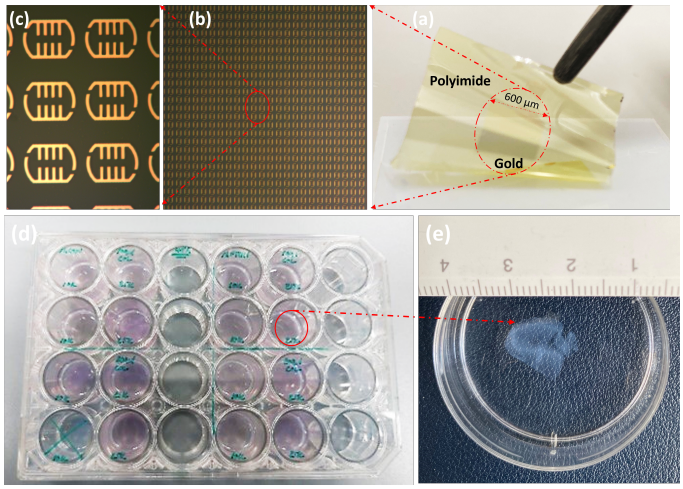

Fig. 2: (a) Demonstration of the flexibility of the biosensor. (b-c) fabricated metasurface biosensor under an optical microscope, (d) cultured 3D collagen gel models of BCC in 24-well plates, and (e) a close-up view.

any change in the transmission spectra can only can only be associated with the alteration of the external dielectric environment [35]. At the frequency of f_3, Fig 4. (d), radiation losses are dominant, and transmission transparency disappears, leading to reforming of electric dipole and a weaker out-phase current distribution that results in an incomplete current.

To provide a quantitative description of the plasmonic EIT-like effect in the metasurface system, the coupled harmonic oscillators model is used to explain the interference between the bright and dark resonators. The charge displacement differential equation of the bright resonator (x_1) indicated by Eq. 1 that interacts with the external electric field E_0 and the charge displacement differential equation of the dark resonator (x_2 by Eq. 2) is given by [36], [37]:

$$\ddot{x}_1(t) + \gamma_1 \dot{x}_1(t) + \omega_0^2 x_1(t) + \kappa x_2(t) = qE_0 \qquad (1)$$

$$\ddot{x}_2(t) + \gamma_2 \dot{x}_2(t) + (\omega_0 + \delta)^2 x_2(t) + \kappa x_1(t) = 0 \qquad (2)$$

Where ω_0 is the resonance frequency of the bright resonator, δ is the detuning factor that represents the frequency difference between peak frequency and the resonance frequency of the bright resonator, γ_1 and γ_2 are the damping rate of the bright and dark resonators, respectively, q is the ratio of the effective charge and mass of the bright mode that quantifies the effective coupling of the bright mode to the external excitation, and κ is the coupling strength between the bright and dark resonators. With the approximation of $\omega - \omega_0 << \omega_0$ and therefore $\omega_0^2 - \omega^2 \cong -2\omega_0(\omega - \omega_0)$ and also assuming that damping rates of the resonators satisfy $\gamma_2 << \gamma_1 << \omega_0$ and a small detuning of $\delta << (\gamma_1, \gamma_2, \kappa)$, the susceptibility is proportional to polarization (P) and can be considered as :

$$\chi_{eff} \propto \frac{(\omega - \omega_0 - \delta) + i\frac{\gamma_2}{2}}{(\omega - \omega_0 + i\frac{\gamma_1}{2})(\omega - \omega_0 - \delta + i\frac{\gamma_2}{2}) - \frac{\kappa^2}{4}} \qquad (3)$$

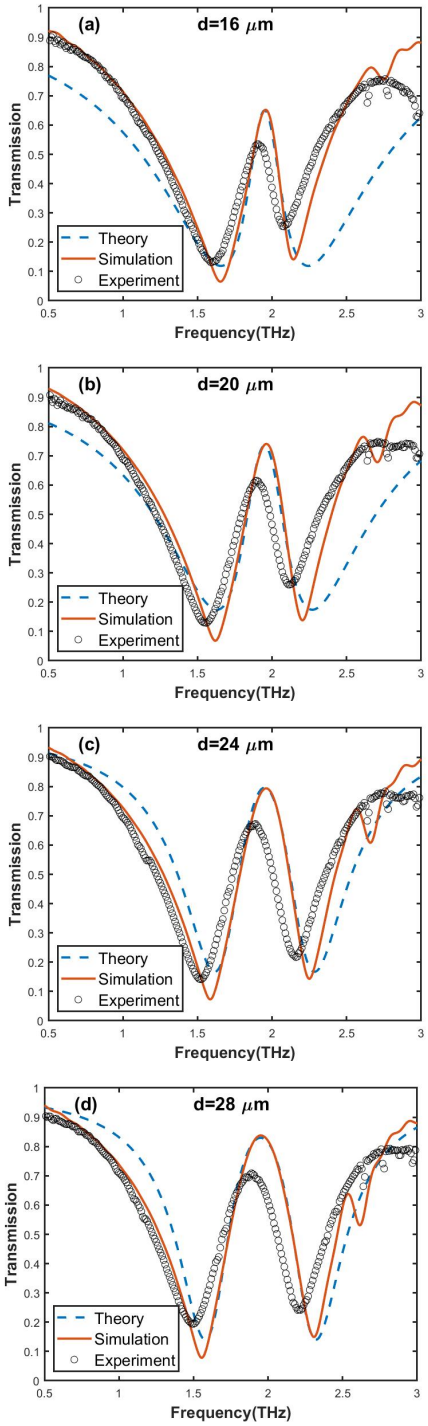

Fig. 3: The transmission spectra of the designed structure as measured (black circle) and simulated (brown line), as well as the theoretical analysis (blue dash line) derived from the coupled oscillator model for (a) $d = 16\ \mu m$, (b) $d = 20\ \mu m$, (c) $d = 24\ \mu m$ and (d) $d = 28\ \mu m$.

The energy loss is proportional to the imaginary part of the susceptibility; thus, given by the Kramers-Kronig relations, the transmission can be written as $T \propto 1 - \chi_i = (1 - q\chi_i)$ which is derived from the conservation of energy relation $T + A = 1$. The obtained transmission with four different

asymmetry levels of $d = (16, 20, 24, 28)\mu m$ analytically fitted according to Eq. 3, which is illustrated by the blue dashed line in Fig. 3 (a-d). As can be observed, the analytically fitted results are in relatively good agreement with both the EM simulation and measured data. According to Fig. 5, with increasing the asymmetry level from 16 to 28 μm, radiation damping of γ_1 decreases from 10.1 to 4.5 THz, and the coupling coefficient improves from 3.3 to 4.5 THz^2, resulting in the intensifying trend of EIT-like resonance. According to the assumption that increasing the degree of asymmetry leads to improved coupling and decreased radiation losses, the transmission peak climbs higher and becomes more sensitive to changes in the local dielectric environment. Additionally, the detuning factor is kept within a narrow range while γ_2 grows from 0.65 to 0.9.

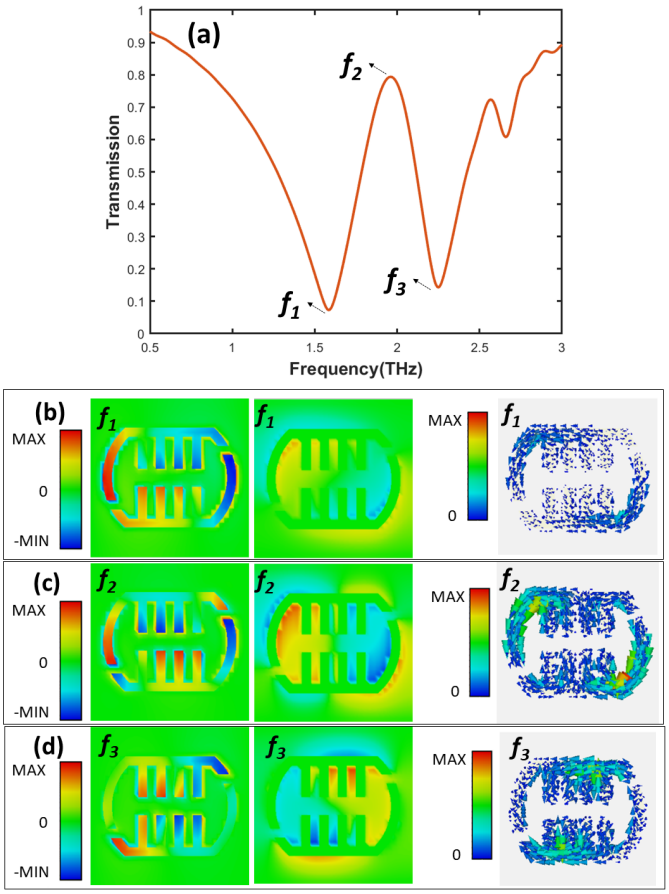

Fig. 4: (a) Simulated transmission spectra. Corresponding electric fields (left), magnetic fields (middle), and surface currents (right) of the designed EIT-like metasurface associated with (b) first dip of $f_1 = 1.58$ THz (c) peak of $f_2 = 1.96$ THz (d) second dip of $f_3 = 2.25$ THz.

Metasurface sensing capabilities often refer to the ability to detect the refractive index of the sample. It is characterized by theoretical sensitivity as $S = \frac{\Delta f}{\Delta n}$ in which Δf is the peak resonance frequency shift corresponding to Δn as the variation of the refractive index. Higher sensitivity refers to larger resonance frequency shift to the permittivty changes on its surface.

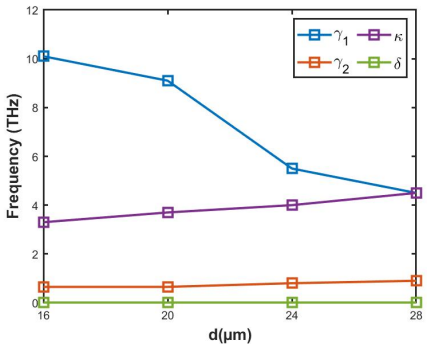

Fig. 5: Extracted damping rates of γ_1 (THz), γ_2 (THz), coupling coefficient of κ (THz^2) and detuning factor of δ (THz) according to analytically fitted curves of coupled oscillator model for different asymmetry values of d.

The greater Q-factor that results in field enhancement depend on the narrower FWHM. In the current work, we have looked into how the FWHM of transmission spectra might be used to track changes in sample characteristics. On the other hand, the the amplitude of the transmission peak varies based on the concentration of cancerous cells and can be a suitable criterion for checking the performance of the biosensor.

Based on these explanations, we have simulated samples of different refractive index, thickness, loss tangent, and occupancy percentage over the metasurface surface. The corresponding resonance frequency shift (Δf), FWHM, and transmission magnitude variation can be seen in Fig. 6-7.

In the simulation, a sample layer with a fixed thickness of 13 μm was placed over the metallic layer, and its refractive index was changed from 1 to 1.9. A linear shift in the EIT-like resonance to the lower frequencies is visible, as shown in Fig. 6. (a) and Fig. 7. (a). The peak frequency shifts from 1.96 THz to 1.62 THz when the refractive index increases from 1 (no sample) to 1.6, giving a notable theoretical sensitivity of 550 GHz/RIU (RIU is the unit of refractive index). According to Fig. 7. (a), the FWHM of the bare sensor is determined to be 382 GHz, and as the refractive index is increased, the FWHM linearly decreases toward 280 GHz for the refractive index of 1.9. Compared to previously investigated EIT-like metasurfaces for cancer sensing, the observed theoretical sensitivity and Q-factor are enhanced [27], [28].

Fig. 6. (b) shows how the thickness of the sample affects the transmission spectra. The resonance frequency shift decreases non-linearly as the thickness of the sample with a fixed refractive index of 1.6 increases from 1 to 13 μm. It can be seen that the sensor response saturates beyond a thickness of thickness of 10 μm and remains unchanged after 13 μm. The localized EM fields that are restricted to the surface region are the cause of this saturation. Fig. 7. (b). also shows that the FWHM similarly decreases from 382 toward 312 GHz for the bare sensor and 13 μm sample, respectively.

Furthermore, a key factor affecting the characteristics of the tumor cells is dissipation loss. Therefore, with a fixed refractive index of 1.6 and a thickness of 13 μm, we changed

the sample loss tangent, ranging from 0 for the bare sensor to 0.25, and observed a significant difference in the transmission magnitude and FWHM. The transmission peak magnitude decreases from 0.82 to 0.51 for loss tangents of 0 and 0.25, respectively, as shown in Fig. 6. (c) and 7. (c). On the other hand, FWHM dramatically increased over the same loss tangent interval, going from 315 to 410. The analysis of transmission peak magnitude and the corresponding FWHM provide key information in characterizing biological samples, including tumor cells.

As a further step toward studying various sample characteristics, we have also investigated the effect of the sample occupancy percentage over the metasurface, as can be seen in Fig. 6. (d) and Fig. 7. (d). It can be concluded that with a redshift, the Δf increases from 165 GHz to 330 GHz by extending the sample coverage area from 25% to 100% while the FWHM reduces from 380 to 312 GHz. The decreasing trend of FWHM with increasing sample coverage area can be explained by the fact that sample absorbs more of the incident EM waves leading to suppressing radiation losses and narrower transmission linewidth.

Based on the sensing capabilities indicated, we investigated the designed metasurface's performance for skin cancer characterization. The ability to distinguish between cancerous and healthy cells and the response to various tumor cell concentrations significantly improve early diagnosis and pharmaceutical treatment of cancer and have been considered in the current study.

The most common type of skin cancer, BCC, was chosen for this work. We then performed qPCR for PTCH1 and housekeeping genes GAPDH and β-Actin to confirm that NEB1-shPTCH1 cells retain their suppressed PTCH1 levels and found that qPCR Ct values were similar to our previous experiments [38] [39]. The cells were cultured in a 6-well plate up to 1×10^5 and 4×10^5 cell numbers were assessed in terms of proliferation (Fig. 8). With a cell density of 4×10^5 cells, NEB1-shCON cells grow to confluency at 24 hours and due to the lack of surface space, the cells are smaller as they are tightly packed together. NEB1-shPTCH1 cells become tightly packed as they become more confluent but as they proliferate slower than NEB1-shCON cells, this is less evident at 24 hours. NEB1-shPTCH1 cells developed a BCC-like phenotype after at least four days of culture and at a lower confluency (Fig. 8. (b).).

With confluency, the behaviour of the cells will change in a number of ways. Therefore, we used a 3D collagen-based model to test with the metasurface biosensor. This allowed us to culture large numbers of cells in a system that allows for vertical growth. If they reach horizontal confluency, the cells would be allowed to continue growing in layers similar to normal skin growth. Another reason for this decision was that we could culture many gels in separate wells and then lift them onto the biosensor for reading, which would be impossible with a monolayer of cells and also in consideration of the cell phenotype as they reach confluency. The cells then can be fixed and dehydrated using 70% ethanol to remove excess water.

For the measurements, we set a time point of 48 hours;

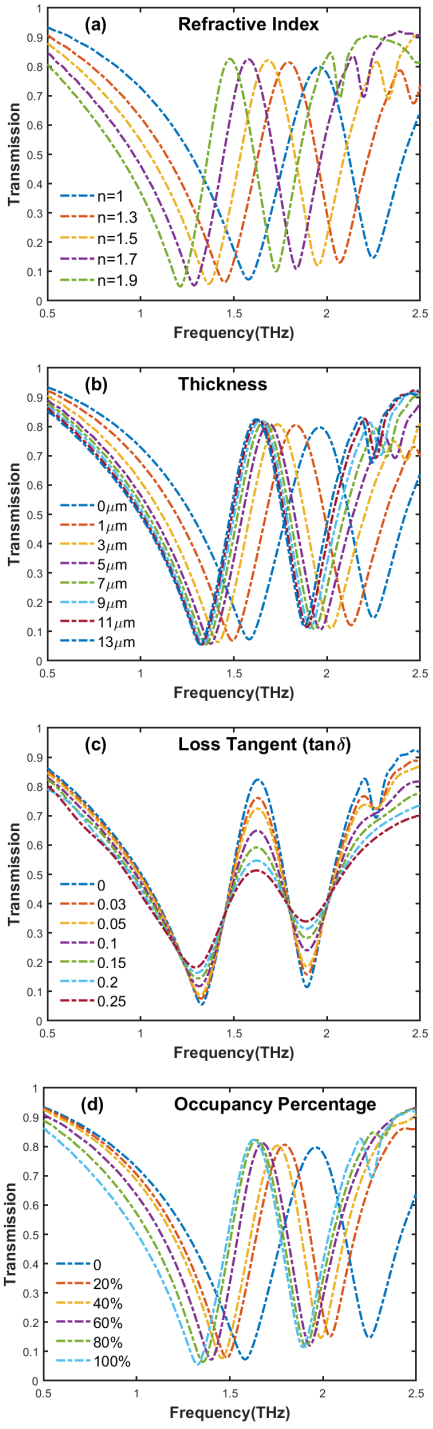

Fig. 6: Transmission spectra variation of the metasurface biosensor based on (a) simulated sample with a refractive index ranging from 1 to 1.9 and a fixed thickness of 13 μm. (b) simulated sample with the thickness increasing from 0 to 13 μm under the fixed refractive index of 1.6. (c) simulated sample with various loss tangents from 0 to 0.25 and a refractive index of 1.6 and thickness of 13 μm (d) simulated sample with the various occupancy area increasing from 0 to 100% with a fixed refractive index of 1.6 and a thickness of 13 μm.

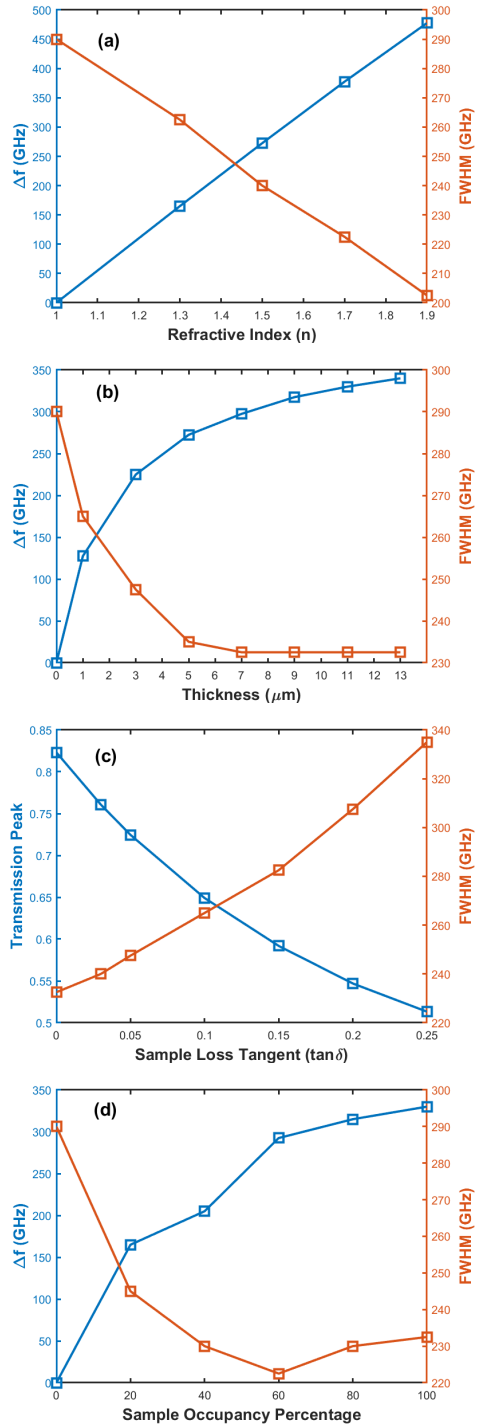

Fig. 7: (a) The resonance frequency and FWHM variation for varying refractive index of sample associated with Fig. 6. (a). (b) The resonance frequency and FWHM variation for varying the thickness of sample associated with Fig. 6. (b). (c) The transmission peak magnitude and FWHM variation for varying loss tangent of sample associated with Fig. 6. (c). (d) The resonance frequency and FWHM variation for varying occupancy percentage of sample associated with Fig. 6. (d).

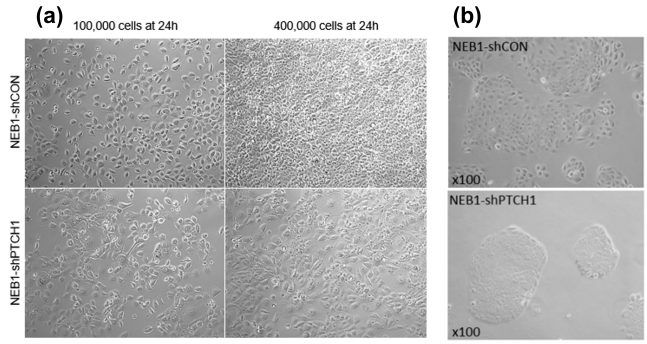

Fig. 8: Proliferation of NEB1 cells cultured in a 6-well plate and (a) cell morphology of the cultured cells after 24 hours. (b) Morphology of NEB1-shCON and NEB1-shPTCH1 cells cultured in normal, lower density, for 4 days.

therefore, this would not be long enough for differentiation, negating the need for fibroblasts or Matrigel. A brief illustration of sample preparation as explained comprehensively in section II is presented in Fig. 10. (a). Gels were made with the thickness of $200\mu l$ collagen I (Fig. 10. (a). (1)) and then Keratinocytes added to the top of the gel with two different cell densities of 1×10^5 and 2.5×10^5 (Fig. 10. (a). (2)). Next, model cultured for 48 hours in a 24-well plate cell culture medium (Fig. 10. (a). (3)). Both cell types of NEB1-shCON (normal keratinocyte) and NEB1-shPTCH1 (BCC) were used, and each gel combination was repeated in triplicate. At the end of the culture period, gels were cut away from the walls of the well plate and washed with PBS. Then, they were fixed in 70% ethanol for 1 hour and at 4°c to ensure that all cells within the gel could be fixed. Finally, all samples were stored in PBS and at 4°c until reading with the biosensor (Fig. 10. (a). (4)).

To ensure accuracy and comparability, each sample underwent treatment by soaking in ethanol to eliminate PBS residue. The biosensor was also washed with ethanol and air-dried before each measurement. The process of placing sample on the metasurface biosensor is depicted in Fig. 10. b. First, every sample was placed onto the periodic metallic resonators (Fig. 10. b. (2)) and then the entire area covered with an extremely narrow, low-density, and stretched Polytetrafluoroethylene (PTFE) film (Fig. 10. b. (3)). This step is crucial in maintaining the sample's consistency across the entire surface and preventing potential air gaps between the biosensor and the sample. PTFE, known for its near transparency in THz frequencies [39], further ensures accurate measurements. Finally, the biosensor and loaded sample were affixed to a sample holder already positioned perpendicular to the direction of the incident wave in the THz-TDS.

Fig. 9 shows the experimental transmission spectra obtained from THz-TDS. We can observe a red shift in the transmission peak of the empty sensor by placing the sample on the metasurface's surface. It is visible that the bare sensor exhibits an EIT-like resonance at 1.88 THz with a transmission peak magnitude of 0.67 and FWHM of 350 GHz. We observe a shift to 1.74 THz, corresponding to a resonance frequency

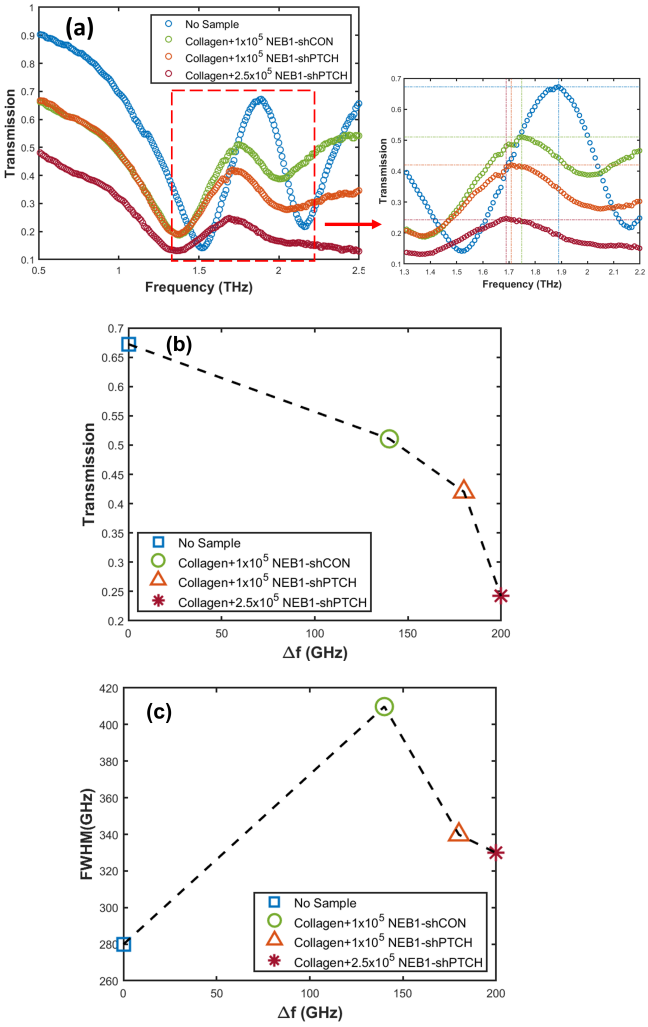

Fig. 9: (a) Measured transmission spectra of the empty biosensor (blue circle), normal cultured skin including $200\mu l$ of collagen and 1×10^5 cell concentration of NEB1-shCON as the model of healthy keratinocyte cell line (green circle), BCC including $200\mu l$ of collagen and 1×10^5 cell concentration of NEB1-shPTCH as the model of BCC cell line (orange circle) and BCC including $200\mu l$ of collagen and 2.5×10^5 cell concentration of NEB1-shPTCH (red circle). (b) Transmission peak magnitude and frequency shift of the corresponding samples. (c) FWHM and frequency shift of the corresponding samples.

shift of 140 GHz, when we add normal cells, containing $200\mu l$ of collagen and 1×10^5 of the healthy keratinocyte cell line of NEB1-shCON. In Fig.9. (b-c), transmission magnitude and FWHM variation have been calculated. For the sample of the healthy keratinocyte cell line, the magnitude falls to 0.51, and FWHM increases to 440 GHz. According to the simulation results shown in Fig. 7. (c), the widening linewidth can be attributed to the collagen gel's rising loss tangent.

By substituting the analyte with the same quantity of collagen and 1×10^5 of NEB1-shPTCH, expressing BCC cell lines, the resonance frequency was further decreased to the point of

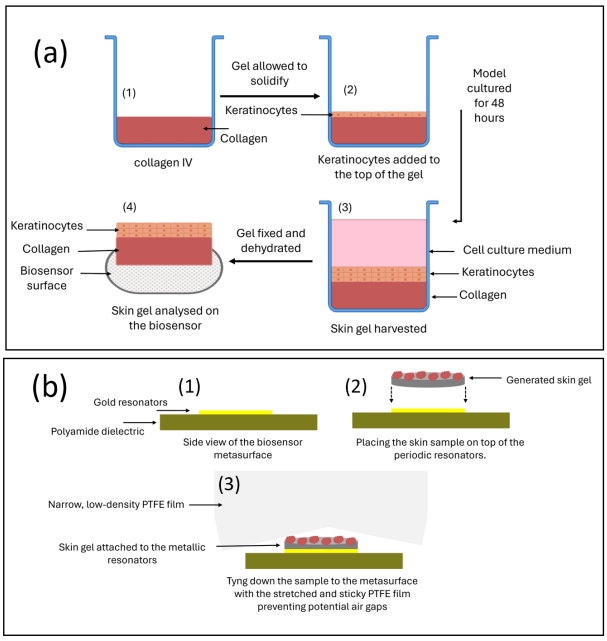

Fig. 10: (a) illustration of Cell Culture Phases (b) The steps of placing sample on the metasurface biosensor

1.70 THz, resulting in Δf of 180 GHz. This finding confirms the ability of the biosensor to distinguish between cancerous and healthy cells based on their permittivity and contributes to the understanding of the relationship between cell types and resonance peak shifts. On the other hand, FWHM drops somewhat to 389 GHz while the transmission magnitude drops further to 0.42. The changes in transmission and FWHM indicated for the same number of normal and malignant cells can also be linked to differences in the morphology of the two stem cell lines shown in Fig. 8. (a-b). Consequently, we see a resonance frequency shift to 1.68 THz and a Δf of 200 GHz compared to a bare sensor when the concentration of BCC cell lines is increased to 2.5×10^5. A relationship between the concentration of tumor cells and the EIT-like resonance can be established with this resonance frequency shift, which can also offer an alternative way to investigate the activity of cancer cells. In this case, we see higher transmission drops than the BCC with the lower concentration, measured at 0.24, and FWHM again experiences a minor decline, this time with a value of 359 GHz. The same transmission linewidth fluctuation between the simulation and experimental data shows that more cells can more efficiently absorb THz waves, which lowers the radiation losses produced by metallic patterns. On the other hand, the variation of transmission magnitude represented in Fig. 9 also could be associated with the characteristic attribute of tumor cells. The water content of cancerous cells is higher than that of normal cells of similar origin. Due to the high absorption of THz waves by hydrogen bonds of water, cancer cells can be differentiated from normal cells [40]. The fundamental process of carcinogenesis is the continual rise in cell hydration caused by subsequent cancer mutations, and the degree of cell hydration increases with the degree of malignancy [41]. The same interpretation has been observed

in ref [2], [42] for THz spectroscopy of BCC tissue.

As a result, based on the study of normal and cancerous cells, it is found that the introduced combined analysis of three sensing features, including resonance frequency shift, FWHM, and transmission peak magnitude detected by the metasurface biosensor, can differentiate normal cells from BCC and also can react to different concentrations of BCC cells. The finding may help provide a simple, fast, low-cost and flexible biosensor by increasing the effectiveness of BCC detection in the early stages.

IV. Conclusion

In summary, we demonstrated a flexible THz metasurface biosensor consisting of asymmetric resonators on an ultra-thin and flexible dielectric polymer to induce high Q-factor EIT-like resonance for BCC detection. In the frame of numerical studies and theoretical analysis based on a coupled oscillator model, we reported experimental verification of bright-dark modes coupling at 1.96 THz for four asymmetry levels. The unique design and ultra-thin dielectric substrate helped to suppress radiation losses, giving rise to a transparent window with a smaller line width. A detailed investigation including both conventional refractive index and also transmission magnitude and FWHM produced enhanced theoretical sensitivity of 550 GHz/RIU. We cultured 3D collagen gel models of skin with normal keratinocytes and BCC cell line to evaluate biosensor performance in discriminating between normal and BCC cells. This is a significant advance on the earlier research that solely dealt with varying concentrations of cancerous cells. Additionally, the biosensor's ability to detect higher BCC cell numbers was studied, and the related resonance frequency shift, transmission magnitude, and FWHM variation were examined. The presented work promises to help make early skin cancer screening quicker, easier and less expensive.

Acknowledgment

This research was supported by the School of EECS and the Centre for Cell Biology and Cutaneous Research of Bilzard Institute at the Queen Mary University of London.

References

[1] H. D. Heibel, L. Hooey, and C. J. Cockerell, "A review of noninvasive techniques for skin cancer detection in dermatology," *American journal of clinical dermatology*, vol. 21, no. 4, pp. 513–524, 2020.

[2] V. P. Wallace, A. J. Fitzgerald, E. Pickwell, R. J. Pye, P. F. Taday, N. Flanagan, and T. Ha, "Terahertz pulsed spectroscopy of human basal cell carcinoma," *Applied spectroscopy*, vol. 60, no. 10, pp. 1127–1133, 2006.

[3] S. Nourinovin, M. M. Rahman, R. C. Jones, M. P. Philpott, and A. Alomainy, "Impact of drug treatment on the electromagnetic properties of basal cell carcinoma cancer in the terahertz band," in *2022 16th European Conference on Antennas and Propagation (EuCAP)*. IEEE, 2022, pp. 1–4.

[4] R. I. Stantchev, X. Yu, T. Blu, and E. Pickwell-MacPherson, "Real-time terahertz imaging with a single-pixel detector," *Nature communications*, vol. 11, no. 1, pp. 1–8, 2020.

[5] L. Yu, L. Hao, T. Meiqiong, H. Jiaoqi, L. Wei, D. Jinying, C. Xueping, F. Weiling, and Z. Yang, "The medical application of terahertz technology in non-invasive detection of cells and tissues: opportunities and challenges," *RSC advances*, vol. 9, no. 17, pp. 9354–9363, 2019.

[6] M. Beruete and I. Jáuregui-López, "Terahertz sensing based on metasurfaces," *Advanced Optical Materials*, vol. 8, no. 3, p. 1900721, 2020.

[7] S. Zhang, C. L. Wong, S. Zeng, R. Bi, K. Tai, K. Dholakia, and M. Olivo, "Metasurfaces for biomedical applications: imaging and sensing from a nanophotonics perspective," *Nanophotonics*, vol. 10, no. 1, pp. 259–293, 2021.

[8] K. Yang, J. Li, M. L. de la Chapelle, G. Huang, Y. Wang, J. Zhang, D. Xu, J. Yao, X. Yang, and W. Fu, "A terahertz metamaterial biosensor for sensitive detection of micrornas based on gold-nanoparticles and strand displacement amplification," *Biosensors and Bioelectronics*, vol. 175, p. 112874, 2021.

[9] X. Deng, Y. Shen, B. Liu, Z. Song, X. He, Q. Zhang, D. Ling, D. Liu, and D. Wei, "Terahertz metamaterial sensor for sensitive detection of citrate salt solutions," *Biosensors*, vol. 12, no. 6, p. 408, 2022.

[10] X. Hu, G. Xu, L. Wen, H. Wang, Y. Zhao, Y. Zhang, D. R. Cumming, and Q. Chen, "Metamaterial absorber integrated microfluidic terahertz sensors," *Laser & Photonics Reviews*, vol. 10, no. 6, pp. 962–969, 2016.

[11] D. Li, S. Lin, F. Hu, Z. Chen, W. Zhang, and J. Han, "Metamaterial terahertz sensor for measuring thermal-induced denaturation temperature of insulin," *IEEE Sensors Journal*, vol. 20, no. 4, pp. 1821–1828, 2019.

[12] S. Park, S. Cha, G. Shin, and Y. Ahn, "Sensing viruses using terahertz nano-gap metamaterials," *Biomedical optics express*, vol. 8, no. 8, pp. 3551–3558, 2017.

[13] S. Xiao, T. Wang, T. Liu, C. Zhou, X. Jiang, and J. Zhang, "Active metamaterials and metadevices: a review," *Journal of Physics D: Applied Physics*, vol. 53, no. 50, p. 503002, 2020.

[14] S. Nourinovin, M. M. Rahman, M. P. Philpott, and A. Alomainy, "Terahertz characterisation of artificially cultured oral cancer with stem cell lines for healthcare applications," in *2022 IEEE International Symposium on Medical Measurements and Applications (MeMeA)*. IEEE, 2022, pp. 1–5.

[15] Z. Zhang, M. Yang, X. Yan, X. Guo, J. Li, Y. Yang, D. Wei, L. Liu, J. Xie, Y. Liu *et al.*, "The antibody-free recognition of cancer cells using plasmonic biosensor platforms with the anisotropic resonant metasurfaces," *ACS applied materials & interfaces*, vol. 12, no. 10, pp. 11 388–11 396, 2020.

[16] W. Fang, X. Lv, Z. Ma, J. Liu, W. Pei, and Z. Geng, "A flexible terahertz metamaterial biosensor for cancer cell growth and migration detection," *Micromachines*, vol. 13, no. 4, p. 631, 2022.

[17] L. Liu, T. Li, Z. Liu, F. Fan, H. Yuan, Z. Zhang, S. Chang, and X. Zhang, "Terahertz polarization sensing based on metasurface microsensor display anti-proliferation of tumor cells with aspirin," *Biomedical Optics Express*, vol. 11, no. 5, pp. 2416–2430, 2020.

[18] M. Yang, Z. Zhang, X. Yan, L. Liang, D. Wei, L. Liu, Y. Ye, Y. Ren, X. Ren, and J. Yao, "The biosensing of liver cancer cells based on the terahertz plasmonic metamaterials," in *Infrared, Millimeter-Wave, and Terahertz Technologies VI*, vol. 11196. International Society for Optics and Photonics, 2019, p. 111960E.

[19] D. Conteduca, I. Barth, G. Pitruzzello, C. P. Reardon, E. R. Martins, and T. F. Krauss, "Dielectric nanohole array metasurface for high-resolution near-field sensing and imaging," *Nature communications*, vol. 12, no. 1, pp. 1–9, 2021.

[20] X. Yan, T. Li, G. Ma, J. Gao, T. Wang, H. Yao, M. Yang, L. Liang, J. Li, J. Li *et al.*, "Ultra-sensitive dirac-point-based biosensing on terahertz metasurfaces comprising patterned graphene and perovskites," *Photonics Research*, vol. 10, no. 2, pp. 280–288, 2022.

[21] C. Zhang, T. Xue, J. Zhang, L. Liu, J. Xie, G. Wang, J. Yao, W. Zhu, and X. Ye, "Terahertz toroidal metasurface biosensor for sensitive distinction of lung cancer cells," *Nanophotonics*, 2021.

[22] R. Singh, W. Cao, I. Al-Naib, L. Cong, W. Withayachumnankul, and W. Zhang, "Ultrasensitive terahertz sensing with high-q fano resonances in metasurfaces," *Applied Physics Letters*, vol. 105, no. 17, p. 171101, 2014.

[23] L. Cong, M. Manjappa, N. Xu, I. Al-Naib, W. Zhang, and R. Singh, "Fano resonances in terahertz metasurfaces: a figure of merit optimization," *Advanced Optical Materials*, vol. 3, no. 11, pp. 1537–1543, 2015.

[24] L. Zhu and L. Dong, "Electromagnetically induced transparency metamaterials: theories, designs and applications," *Journal of Physics D: Applied Physics*, vol. 55, no. 26, p. 263003, 2022.

[25] T. Lin, Y. Huang, S. Zhong, Y. Zhong, Z. Zhang, Q. Zeng, Y. Yu, and Z. Peng, "Field manipulation of electromagnetically induced transparency analogue in terahertz metamaterials for enhancing liquid sensing," *Optics and Lasers in Engineering*, vol. 157, p. 107127, 2022.

[26] M. Yang, L. Liang, Z. Zhang, Y. Xin, D. Wei, X. Song, H. Zhang, Y. Lu, M. Wang, M. Zhang *et al.*, "Electromagnetically induced transparency-like metamaterials for detection of lung cancer cells," *Optics express*, vol. 27, no. 14, pp. 19 520–19 529, 2019.

[27] X. Yan, M. Yang, Z. Zhang, L. Liang, D. Wei, M. Wang, M. Zhang, T. Wang, L. Liu, J. Xie *et al.*, "The terahertz electromagnetically induced

transparency-like metamaterials for sensitive biosensors in the detection of cancer cells," *Biosensors and Bioelectronics*, vol. 126, pp. 485–492, 2019.

[28] J. Zhang, N. Mu, L. Liu, J. Xie, H. Feng, J. Yao, T. Chen, and W. Zhu, "Highly sensitive detection of malignant glioma cells using metamaterial-inspired thz biosensor based on electromagnetically induced transparency," *Biosensors and Bioelectronics*, vol. 185, p. 113241, 2021.

[29] Z. Zhang, H. Ding, X. Yan, L. Liang, D. Wei, M. Wang, Q. Yang, and J. Yao, "Sensitive detection of cancer cell apoptosis based on the non-bianisotropic metamaterials biosensors in terahertz frequency," *Optical Materials Express*, vol. 8, no. 3, pp. 659–667, 2018.

[30] D. Seliuta, G. Šlekas, A. Kamarauskas, and Ž. Kancleris, "Guided lattice modes in terahertz metasurface deposited on ultrathin dielectric substrate," *IEEE Transactions on Terahertz Science and Technology*, 2022.

[31] H. Yao, H. Mei, W. Zhang, S. Zhong, and X. Wang, "Theoretical and experimental research on terahertz metamaterial sensor with flexible substrate," *IEEE Photonics Journal*, vol. 14, no. 1, pp. 1–9, 2021.

[32] M. M. Rahman, A. Hazan, J. L. Selway, D. S. Herath, C. A. Harwood, M. S. Pirzado, R. Atkar, D. P. Kelsell, K. J. Linton, M. P. Philpott *et al.*, "A novel mechanism for activation of gli1 by nuclear smo that escapes anti-smo inhibitors," *Cancer Research*, vol. 78, no. 10, pp. 2577–2588, 2018.

[33] V. Fedotov, M. Rose, S. Prosvirnin, N. Papasimakis, and N. Zheludev, "Sharp trapped-mode resonances in planar metamaterials with a broken structural symmetry," *Physical review letters*, vol. 99, no. 14, p. 147401, 2007.

[34] P. Tassin, L. Zhang, R. Zhao, A. Jain, T. Koschny, and C. M. Soukoulis, "Electromagnetically induced transparency and absorption in metamaterials: the radiating two-oscillator model and its experimental confirmation," *Physical review letters*, vol. 109, no. 18, p. 187401, 2012.

[35] J. Wang, C. Fan, J. He, P. Ding, E. Liang, and Q. Xue, "Double fano resonances due to interplay of electric and magnetic plasmon modes in planar plasmonic structure with high sensing sensitivity," *Optics express*, vol. 21, no. 2, pp. 2236–2244, 2013.

[36] C. Garrido Alzar, M. Martinez, and P. Nussenzveig, "Classical analog of electromagnetically induced transparency," *American Journal of Physics*, vol. 70, no. 1, pp. 37–41, 2002.

[37] N. Liu, L. Langguth, T. Weiss, J. Kästel, M. Fleischhauer, T. Pfau, and H. Giessen, "Plasmonic analogue of electromagnetically induced transparency at the drude damping limit," *Nature materials*, vol. 8, no. 9, pp. 758–762, 2009.

[38] S. Nourinovin, M. M. Rahman, M. P. Philpott, Q. H. Abbasi, and A. Alomainy, "Terahertz characterisation of ordinary and aggressive types of oral squamous cell carcinoma as a function of cancer stage and treatment efficiency," *IEEE Transactions on Instrumentation and Measurement*, 2023.

[39] S. Nourinovin, M. M. Rahman, S. J. Park, H. Hamid, M. P. Philpott, and A. Alomainy, "Terahertz dielectric characterisation of three-dimensional organotypic treated basal cell carcinoma and corresponding double debye model," *IEEE Transactions on Terahertz Science and Technology*, 2023.

[40] G. McIntyre, "Cell hydration as the primary factor in carcinogenesis: a unifying concept," *Medical hypotheses*, vol. 66, no. 3, pp. 518–526, 2006.

[41] M. Marques, A. Batista de Carvalho, A. Mamede, A. Dopplapudi, V. García Sakai, and L. Batista de Carvalho, "Role of intracellular water in the normal-to-cancer transition in human cells—insights from quasi-elastic neutron scattering," *Structural Dynamics*, vol. 7, no. 5, p. 054701, 2020.

[42] E. Pickwell, A. J. Fitzgerald, B. E. Cole, P. F. Taday, R. J. Pye, T. Ha, M. Pepper, and V. P. Wallace, "Simulating the response of terahertz radiation to basal cell carcinoma using ex vivo spectroscopy measurements," *Journal of Biomedical Optics*, vol. 10, no. 6, p. 064021, 2005.